Medium-Voltage Converter Solution with Modular Multilevel Structure and Decentralized Energy Storage Integration for High-Power Wind Turbines

Medium-Voltage Converter Solution with Modular Multilevel Structure and Decentralized Energy Storage Integration for High-Power Wind Turbines

Gustavo Gontijo, *Member, IEEE,* Tamas Kerekes, *Senior Member, IEEE,* Dezso Sera, *Senior Member, IEEE,* Mattia Ricco, *Senior Member, IEEE,* Laszlo Mathe, *Senior Member, IEEE,* and Remus Teodorescu, *Fellow, IEEE*

***Abstract*—As the penetration of renewable energy generation increases, the importance of energy storage systems becomes evident since these systems can contribute for the preservation of the power system stability. Wind turbine owners can also benefit from having energy storage systems as they can increase their revenues. The fast growth of wind turbine power ratings will eventually lead to the requirement of higher voltage levels as well. Proper power-electronic converters will be required to drive these systems. Converters with a modular multilevel structure are considered the state-of-the-art solution for high-power applications. These topologies allow for a flexible integration of energy storage systems in both centralized and decentralized ways. This paper presents a new converter solution with a modular multilevel structure and decentralized energy storage integration suitable to drive high-power medium-voltage wind turbines. This converter presents important structural and control characteristics that allows for a straightforward integration of an energy storage system in such a way that the wind turbine driven by it can operate with high flexibility and in a dispatchable fashion, benefiting both the power system operator and the wind-power-plant owner.**

***Index Terms*—modular multilevel converters, wind turbines, energy storage systems.**

I. Introduction

THE world has been facing an increasing penetration of renewable energy sources into the electrical grid, which brings challenges to the operation of power systems. The power systems operate in an on-demand fashion, instantaneously controlling the generation to meet the load and, thus, maintaining frequency stability. Wind turbines (WTs) and solar photovoltaic systems are non-dispatchable generation sources since it is not possible to control the amount of power injected into the grid as it is dependent on the energy resource availability at the given moment. Energy storage systems (ESSs) will be an essential technology to allow for the proper integration of renewable energy sources in the future electrical grids. A wind power plant with an ESS can operate in a dispatchable fashion contributing to the grid frequency regulation and economic dispatch [1], [2]. Besides, the ESS allows the WT to have an inertial response, preserving the grid stability [1], [2]. Finally, the WT with an ESS can help to black start the electrical grid, after a blackout, in a bottom-up approach (starting from the distribution level towards the transmission level), which can considerably reduce the grid restoration time, minimizing the economic losses of the industry [3].

Besides the advantages to the power system operation, WT owners can also benefit from the usage of an ESS. The usage of an ESS can lead to higher revenues in the electricity market [4]. In other words, WT owners sign contracts that are based on generation forecasts and they suffer financial penalties for mismatches between the contracted power and the actual generated power. This problem could be solved with an ESS. Moreover, an ESS could maintain a wind power plant active during a grid fault that would isolate the power plant from the main grid. The ESS converter would operate in a grid-forming mode while absorbing the energy generated by the WTs.

Upscaling is a trend in modern WTs, which aims at building turbines with higher power ratings while reducing structural costs, size and weight [5], [6]. As the power levels of the WTs increase, it is natural to expect an increase of voltage levels of the equipment and devices related to them as well. In fact, it has been proved that, at a certain power level, the usage of a medium-voltage (MV) structure, including generator and power-electronic converter, results in reduced costs, size and weight [7]. A MV structure would reduce the size of the WT transformer or could even lead to a transformer-less operation [8], [9]. The increased voltage levels would reduce the turbine currents, leading to lower losses and leading to a considerable reduction of the size of the turbine cables, which would contribute to a smaller weight of the solution in general [10]. This fact could be very beneficial to offshore WTs that require complex and expensive supporting structures that must be capable to withstand the turbine weight.

The integration of ESSs in wind power plants can be executed in different ways. First, the ESS could be installed at the point of connection of the wind power plant to the grid, in which the ESS would require its own dedicated converter. The ESS could also be integrated into the WT converter. In this paper, batteries are considered as the ESS. However, any other ESS technology, such as supercapacitors, could be adopted if desired. Power-electronic converters with modular multilevel structure allow for both centralized and decentralized integration of batteries [11]–[16]. In the centralized case, the batteries are connected to the converter DC link, whereas in the decentralized one, the batteries are distributed into each converter submodule. Having the batteries integrated into the WT converter could potentially reduce costs and, in general, reduce the size and weight of the wind power plant structure, which could be very beneficial to offshore wind power plants. Besides, the usage of decentralized batteries in the WT allows for battery packs with reduced voltages, with a reduced number of series-connected cells, which simplifies

the control and monitoring of such systems, potentially leading to the requirement of a cheaper battery management system (BMS). Since the applications considered are medium-voltage ones, having the ESS in a centralized manner (connected to the converter DC link) could be a hard task due to the necessity of many series-connected battery cells.

In this paper, a new AC-AC converter solution with a modular multilevel structure and decentralized battery integration is proposed. Due to its simple structure and straightforward control, the proposed solution allows for the safe integration of batteries into the same converter that drives the WT. Due to its modular multilevel structure, the proposed converter topology would be suitable to drive modern high-power medium-voltage WTs. These WTs would operate with high flexibility and in a dispatchable fashion, benefiting both the power system operator and WT owners. Once again, the proposed converter solution presents a straightforward control and modulation, with few internal control loops, which is a considerable advantage in comparison to other well-established modular multilevel converters. For example, undesired circulating currents are non existent in its operation, which avoids the need of a circulating-current suppression control. Moreover, due to the absence of undesired circulating currents and due to the fact that different submodule strings are never connected simultaneously to the same terminal, the proposed converter topology does not require the bulky and heavy arm/string inductors present in other well-established modular multilevel converters. The integration of the ESS into the WT converter prevents the need of extra converters exclusively dedicated to the ESS, contributing to the general weight and cost reduction of the wind power plant. It is important to emphasize that converters with modular multilevel structure and ESS integration operating as independent units capable of providing ancillary services to the electrical grid have been widely discussed in the literature [11]–[14]. However, to the best of the author's knowledge, the application of converters with a modular multilevel structure and ESS integration to drive a MV WT operating with different grid-side and generator-side power set points is a topic rarely or never explored in the literature before, which emphasizes the contribution of this paper. In other words, the converter topology introduced in this paper might be the first solution proposed in the literature capable to drive medium-voltage WTs with ESS integration, operating with different grid-side and generator-side power set points. In this paper, a detailed explanation of the internal operation of the proposed converter topology is provided, including the presentation of the control strategy. Simulation results are presented to demonstrate the operation of the proposed solution driving a MV WT with different grid-side and generator-side power set points. Finally, experimental results are presented to validate important points of the new converter solution proposed in this paper. The paper is structured as follows: The proposed topology and its control are presented in Section II and Section III, respectively. In Section IV and Section V, the simulation and experimental results are shown, respectively. Finally, conclusions are presented in Section VI.

II. Topology Presentation

The converter solution proposed in this paper is illustrated in Fig. 1, as it is an extension of the topology presented in the patent [17]. The authors named it modular multilevel shunt converter (MMSHC). This converter is composed of six strings of full-bridge (FB) submodules along with twelve swap switches. Each FB submodule has its own integrated ESS (batteries in this case). Each phase of the converter is composed of two submodule strings (named X and Y) that operate in a complementary fashion. In other words, while one is connected to the generator (charging), the other is connected to the grid (discharging), maintaining a continuous power flow between the grid and the machine. The swap switches are responsible for changing the connection of the strings that can be connected to both generator terminals and grid terminals in a complementary way.

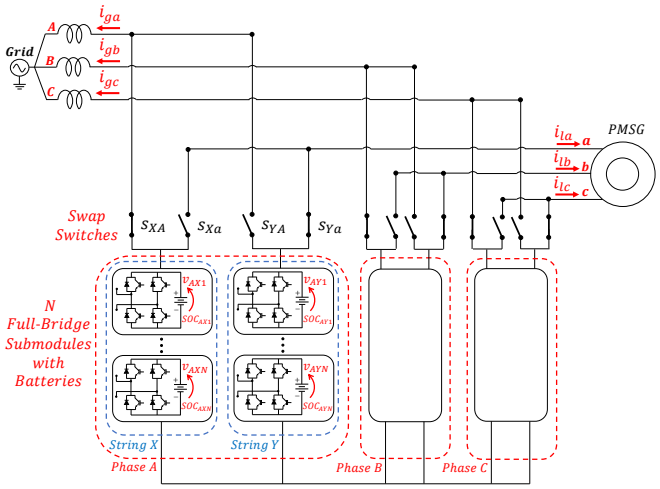

Fig. 1. MMSHC topology.

The MMSHC swap switches operate with an extremely low switching frequency (in a scale of several minutes). In other words, these devices do not switch while the battery state of charge (SOC) remains within a given range, before it reaches a pre-defined limit. For example, when the SOC of the batteries in the charging string reaches the pre-defined upper limit, or the SOC of the batteries in the discharging string reaches the pre-defined lower limit, then the swap switches act, connecting the charging string to the grid terminals and connecting the complementary string, that was discharging at the grid side, to the generator terminals. The MMSHC basic operation is illustrated in Fig. 2 in which each submodule is represented by controlled voltage sources and the converter operation is explained by defining State 1 and State 2. In State 1, String X is connected to the grid (discharging) and String Y is connected to the WT (charging). State 2 is the opposite, which means that String X is connected to the WT (charging) and String Y is connected to the grid (discharging). The MMSHC operates switching, alternately, between these two states. There are two important constraints to be satisfied during the commutation of the swap switches. In Fig. 3, a schematic representation of the MMSHC phase A (see Fig. 1) is shown in which the submodule strings X and Y of the converter are represented as voltage sources and the inductive load is represented as

a current source since its current cannot be instantaneously cut without causing dangerous overvoltages. According to this figure, the commutation constraints become clear. First, the switches S_{XA} and S_{YA} cannot be simultaneously connected to the terminal A and the switches S_{Xa} and S_{Ya} cannot be simultaneously connected to the terminal a. These situations would lead to the short circuit of the two voltage sources that represent the submodule strings X and Y. Second, either the switch S_{Xa} or the switch S_{Ya} must be connected to terminal a at any time (both switches cannot be in off state simultaneously) because the inductive current, represented by the current source, must always have a path to flow through, otherwise serious overvoltages will occur. As previously mentioned, the pairs of switches S_{XA} and S_{Xa}, and S_{YA} and S_{Ya} operate in a complementary fashion (when one is in on state the other is in off state and vice versa). In order to satisfy the commutation constraints, the complementary switches would have to change their switching states instantaneously when the swapping command was given. However, in practice, this is impossible due to small constructive differences among the devices that lead to different turn-on and turn-off times in each of them. Besides, small switching delays could occur due to many different reasons. Thus, some strategy must be adopted to allow for the safe commutation of the MMSHC swap switches.

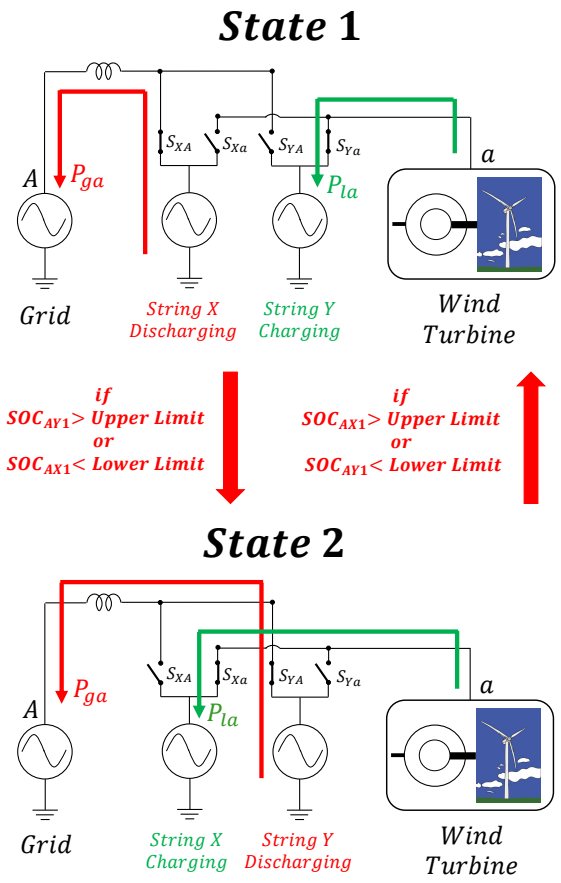

Fig. 2. Basic operation of one phase of the MMSHC.

One of the strategies that can be adopted is the use of a dead-time technique in combination with a given circuit to divert the inductive current during the commutation period. Snubber circuits [18] or diode clamping circuits [19] are examples of circuits that can be used to divert the inductive current during the commutation. The snubber option is illustrated in Fig. 4.

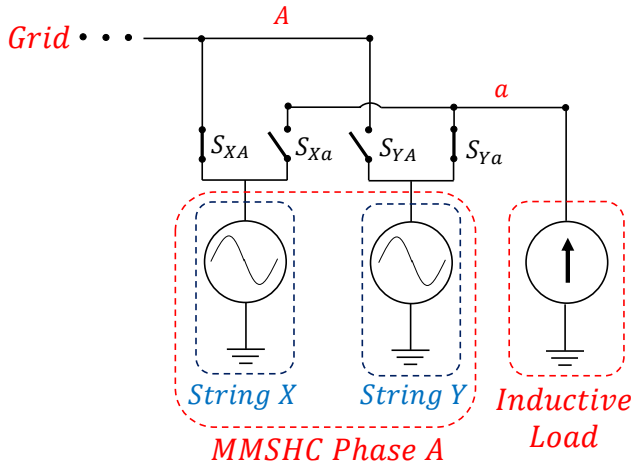

Fig. 3. Schematic representation of the MMSHC phase A that illustrates the swap-switch commutation constraints.

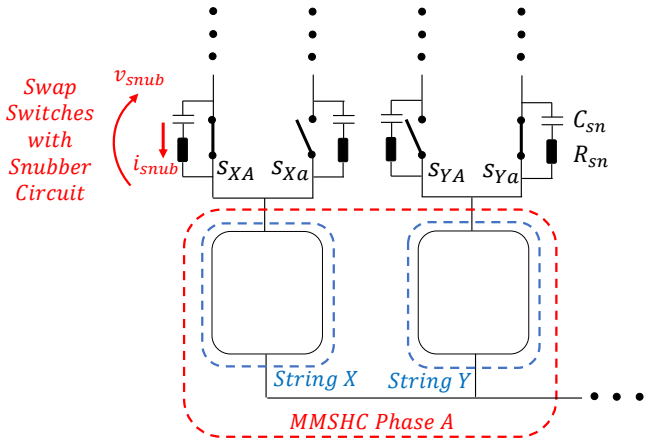

Fig. 4. Illustration of the swap-switch snubber circuit.

If the snubber approach is adopted, when a swapping command is given to the converter, the first step of the commutation process is to give the turn-off command to the swap switches that are in on state. As a second step, a predefined dead-time period should be waited (to guarantee that all the switches turn off before turning other switches on) during which the string current flows through the snubber circuits since all the switches are in off state. Then, the third step of the commutation process is to send the turn-on command to the swap switches to be closed. It is very important to emphasize that, since the operation of the swap switches occurs with a considerably high time constant or extremely low switching frequency (in a scale of several minutes), then the losses caused by the currents flowing through the snubber circuits are quite low. Another issue that might raise some concerns about the swap switches is related to the voltage levels that they must be capable to block. Since medium-voltage levels are considered, the swap switches must be capable to block such considerably high voltages. If semiconductor switches are used, then series-connected

devices might be required depending on the voltage levels. However, due to the extremely low switching frequency, the swap switches could be mechanical ones such as contactors or high-voltage relays along with a snubber circuit. Essentially, the MMSHC swap switches are not high-switching-frequency devices. Instead, they simply change the connection of the submodule strings, between grid and load terminals, in a scale of minutes allowing for the power transfer from the generator to the grid.

Another possibility would be to build the MMSHC swap switches based on semiconductor devices. As illustrated in Fig. 3, the swap switches must be capable to block the voltage difference between two AC voltage sources that represent String X and String Y. In other words, these switches must be capable of blocking voltages with positive and negative polarities and must be capable of conducting current in both directions. The semiconductor-device-based technology capable of performing this task is the bidirectional switch widely applied to the well-established matrix converters [19], [20]. The four-step commutation method [19], [20] is a technique that allows for the bidirectional-switch commutation process, guaranteeing that there is no short circuit between the voltage sources and guaranteeing that there is always a path for the inductive load current to flow trough. This way, the dead-time plus snubber circuit approach, shown in Fig. 4, can be avoided. The four-step commutation method is explained in Fig. 5.

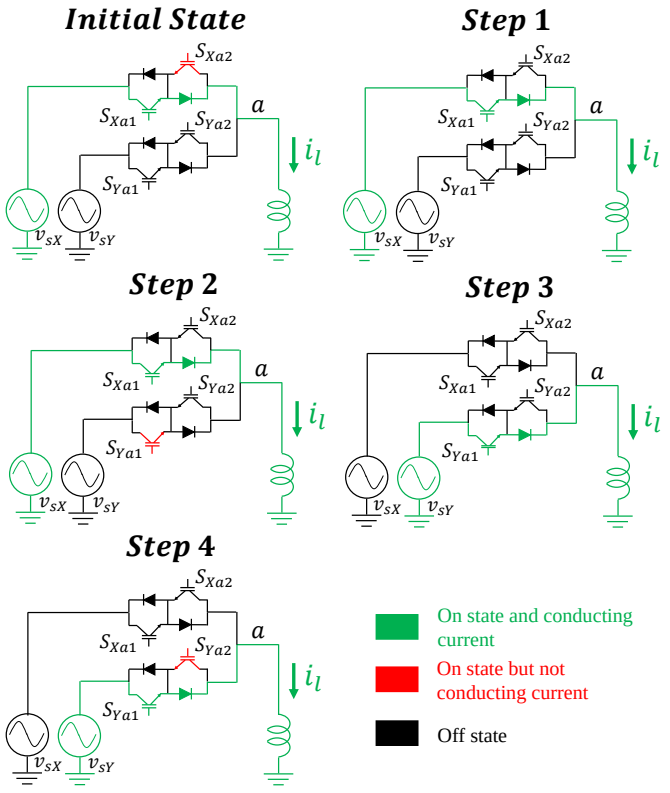

Fig. 5. Explanation of the four-step commutation method.

In Fig. 5, the two voltage sources representing strings X and Y are shown, along with the two bidirectional-switch valves S_{Xa} and S_{Ya} that connect String X and String Y, respectively, to the load terminal (terminal a). In Fig. 5, the green color represents the load current (i_l) path, and it represents the semiconductor devices in on state and conducting current. The red color represents the semiconductor devices in on state but not conducting current. The black color represents the semiconductor devices in off state. The four-step commutation method requires the measurement of the load current since it is based on the current direction that the commutation steps are decided. Let us suppose that the initial state condition and the instantaneous direction of the load current at the moment of the commutation are the ones shown in Fig. 5. In the initial state, both IGBTs S_{Xa1} and S_{Xa2} are in on state, but only S_{Xa1} carries the current due to its instantaneous direction. When a swapping command is given, the four-step commutation process must begin. Step 1 corresponds to turning off the IGBT that is not conducting current in the active bidirectional switch (S_{Xa2}). Step 2 corresponds to turning on the IGBT of the other bidirectional switch, which is capable to conduct the load current with the given instantaneous direction (S_{Ya1} in this case). At this stage, the inductive current is still flowing through S_{Xa1}. In Step 2, it is interesting to notice that even though S_{Xa1} and S_{Ya1} are turned on, their series-connected diodes guarantee that a short circuit between the two voltage sources does not occur. In other words, since the cathode of the diodes are connected to a common point (terminal a), then the diode to conduct the current will be the one with higher anode voltage. If in Step 2 v_{sY} is higher than v_{sX}, then the load current will start to flow through S_{Ya1}. In Step 3, S_{Xa1} is turned off and, thus, the load current naturally starts to flow through S_{Ya1}. Finally, in Step 4, S_{Ya2} is turned on to make sure that when i_l changes direction there is a path for it to flow through.

One issue that deserves special attention when implementing the swap switches based on semiconductor devices is the fact that series-connected devices might be required to be possible to block the medium voltage levels. However, it is important to mention that these are medium-voltage levels and not high-voltage ones and, thus, only a few series-connected devices should be required, especially considering the availability of modern devices with voltage ratings of up to 10 kV [21]. As an example, let us suppose the situation corresponding to Step 2 in Fig. 5. Let us also suppose that v_{sX} and v_{sY} have different frequencies but the same peak value equal to 5 kV. Finally, let us consider that at the moment corresponding to Step 2, v_{sX} is in its peak equal to $+5$ kV and v_{sY} is in its valley equal to -5 kV. Since in Step 2 S_{Ya1} is turned on, then v_{sY} is connected to the mid point of the lower bidirectional switch and v_{sX} is connected to terminal a, which means that the voltage blocked by S_{Ya2} is equal to 10 kV. Since semiconductor devices are typically designed to operate blocking maximum 50 % of their rated voltage, then two series-connected 10-kV semiconductor devices would be required to build S_{Xa1}, S_{Xa2}, S_{Ya1} and S_{Ya2}. Two series-connected devices operating with an extremely low switching frequency should not be a big challenge to implement from a practical point of view.

One of the problems of series-connected semiconductor devices operating with high switching frequency is the poor dynamic voltage sharing among the series-connected devices that might occur during the commutation process, which can

lead to dangerous situations [22]. Another problem is the excessively high switching losses due to the high voltages and currents handled by the semiconductor valves. Those problems would be evident if a two-level three-phase converter were to be used in medium-voltage applications. However, as previously mentioned, the MMSHC swap switches operate with an extremely low switching frequency and, thus, the previously mentioned problems should be nonexistent or at least they could be considerably reduced. Moreover, there are some products currently available in the industry [22] that are valves composed of several series-connected semiconductor devices. These valves can operate in a safe and reliable fashion due to modern drivers that guarantee proper dynamic voltage sharing among the series-connected devices, during the commutation process. This technology could be adopted to build the MMSHC bidirectional-switch valves.

III. MMSHC Internal Control

In Fig. 6, one can observe the internal control and the modulation of phase A of the MMSHC. Each converter phase is independent and operates with this internal control. The control receives as inputs the references of both the grid voltage (v_{ga}^*) and the load voltage (v_{la}^*), coming from outer control loops, the current measured at both grid terminals (i_{ga}) and generator terminals (i_{la}) and the battery SOC of each submodule in each string ($SOC_{AX1}, SOC_{AX2}...SOC_{AXN}$ and $SOC_{AY1}, SOC_{AY2}...SOC_{AYN}$).

As described in Fig. 6, the variables S_{XA} and S_{Xa} are initialized with values equal to 1 and 0 ($S_{XA} = 1$ and $S_{Xa} = 0$), respectively, which means that String X starts connected to the grid terminals (discharging), whereas String Y starts connected to the machine terminals (charging). Two main control objectives are defined for the MMSHC. First, all of its batteries should always operate within a given pre-defined SOC range. Second, the switching frequency of the MMSHC swap switches should be limited in order to avoid losses in the snubber circuits. These two control objectives are achieved with the algorithm described in the flowchart depicted in Fig. 6. The first stage of the MMSHC control is responsible for maintaining the battery-SOC values of the submodules of both strings (X and Y) within a given range. In other words, an upper limit and a lower limit of SOC are predefined and the batteries of all the submodules in both strings should always operate within these limits. Initially, it is necessary to check the connections of each string (which terminal each of the two strings are connected to). In order to do so, the control logic checks the status of the swap switches of String X (if $S_{XA} = 1$ and $S_{Xa} = 0$). If $S_{XA} = 1$ and $S_{Xa} = 0$, then it means that String X is connected to the grid, discharging, and String Y is connected to the generator, charging. In this case, the control logic needs to check if the SOC of the batteries in String Y is higher than the pre-defined upper limit and if the SOC of the batteries in String X is lower than the pre-defined lower limit. One of these two limits will be exceeded first, depending whether the power injected into the grid by the MMSHC is higher or lower than the power being produced by the generator. While these limits are not exceeded, String X is kept connected to the grid terminals (discharging) and String Y is kept connected to the generator terminals (charging). In this case, the swap switches S_{XA}, S_{Xa}, S_{YA} and S_{Ya} receive values equal to $1, 0, 0$ and 1, respectively, in which 0 means off state and 1 means on state. Moreover, the reference value of the voltage that must be synthesized across String X (v_{sX}^*) becomes equal to the grid voltage reference (v_{ga}^*), the reference value of the voltage that must be synthesized across String Y (v_{sY}^*) becomes equal to the generator voltage reference (v_{la}^*), the String X current (i_X) becomes equal to the grid current (i_{ga}) and the String Y current (i_Y) becomes equal to the generator current (i_{la}). If any of the two limits (upper or lower) are exceeded, the swap switches act connecting String X to the generator terminals, and connecting String Y to the grid terminals. In other words, S_{XA}, S_{Xa}, S_{YA} and S_{Ya} receive values equal to $0, 1, 1$ and 0, respectively. This means that String X enters in charging mode and String Y enters in discharging mode. At this moment, the reference value of the voltage that must be synthesized across String X (v_{sX}^*) becomes equal to the generator voltage reference (v_{la}^*), the reference value of the voltage that must be synthesized across String Y (v_{sY}^*) becomes equal to the grid voltage reference (v_{ga}^*), the String X current (i_X) becomes equal to the generator current (i_{la}), the String Y current (i_Y) becomes equal to the grid current (i_{ga}). Now, the control logic needs to check if the SOC of the batteries in String X is higher than the pre-defined upper limit and if the SOC of the batteries in String Y is lower than the pre-defined lower limit. While these limits are not exceeded, String Y is kept connected to the grid terminals (discharging) and String X is kept connected to the generator terminals (charging). As illustrated in Fig. 6, in the first stage of the control, the battery SOCs of submodules number 1 of Strings X and Y (SOC_{AX1} and SOC_{AY1}, respectively) are used to define the swap-switch operation. However, it is important to emphasize that any battery SOC from any submodule in each string could be used since they all have the same value due to the SOC-balancing control. In other words, $SOC_{AX1} = SOC_{AX2} = ... = SOC_{AXN}$ and $SOC_{AY1} = SOC_{AY2} = ... = SOC_{AYN}$. The SOC-balancing control will be explained below.

The second stage of the MMSHC control is responsible for the modulation and SOC-balancing control of the converter submodules. In other words, this is the String X and String Y control. According to Fig. 6, after defining the voltage references and current values for both Strings X and Y, the string control starts. Using the String X control as an example, first it is necessary to test if the voltage that must be synthesized across the string (v_{sX}) has a positive or negative value to decide if the FB submodules must be inserted with positive or with negative polarity. After that, a level-shifted-carrier pulse-width-modulation (LSC-PWM) technique is used to define the number of submodules (M) that must be inserted. Finally, the last step of the string control corresponds to the SOC-balancing control (sorting algorithm) that, depending on the direction of the current (if the instantaneous value of i_X is positive or negative), decides which submodules of the string should be inserted. If this is a charging current, the M submodules with lower battery-SOC values are selected to be inserted. If this is a discharging current, the M submodules

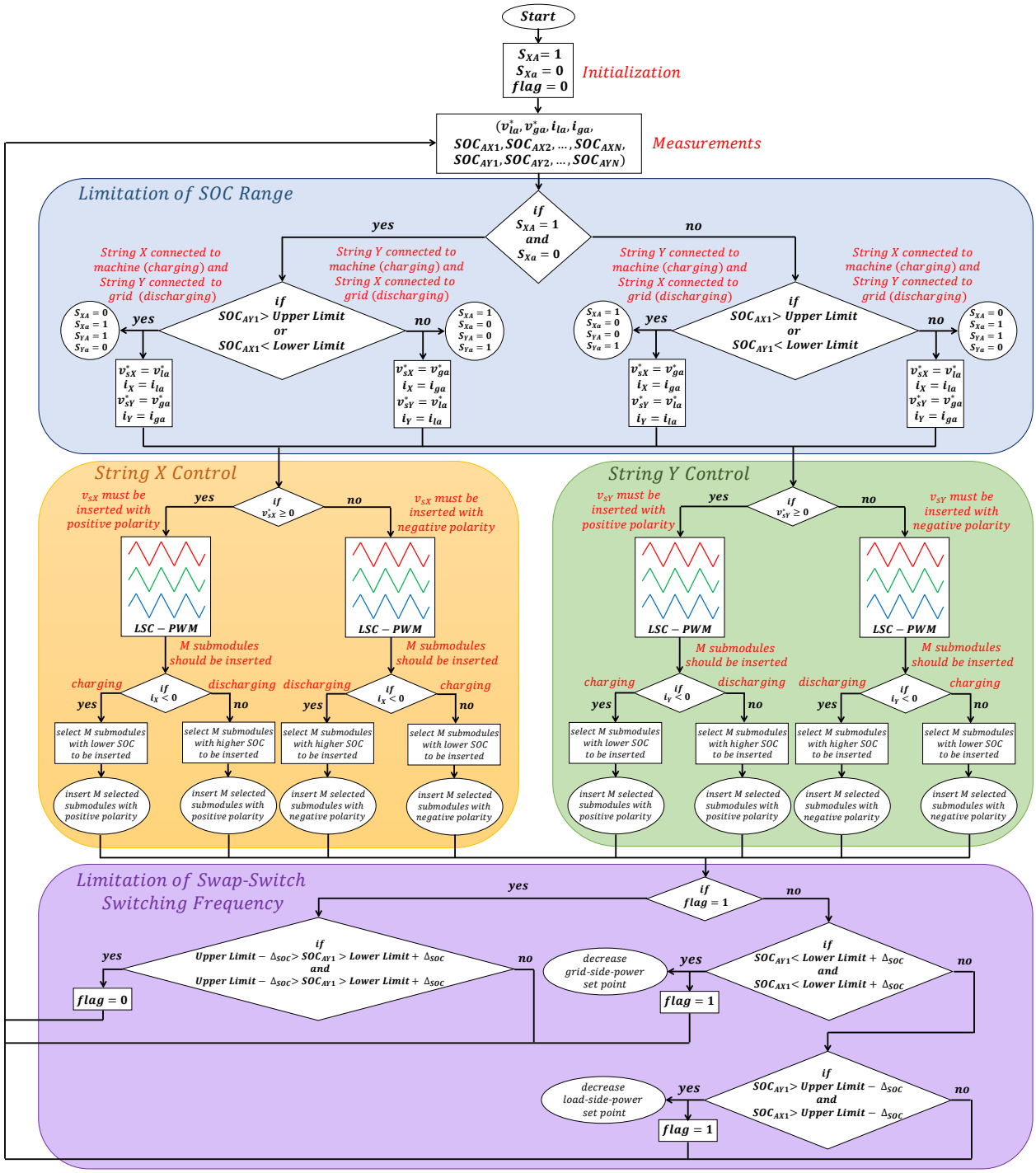

Fig. 6. MMSHC internal control and modulation diagram.

with higher battery-SOC values are selected to be inserted. This control guarantees that the battery-SOC values of all the submodules within the same string remain equal (balanced).

Finally, the last stage of the MMSHC control is responsible for limiting the frequency of operation of the swap switches. Since the amount of energy that can be stored in the batteries is finite, then there is a limit of time in which the power injected into the grid by the MMSHC can be higher than the power being generated by the WT, and this time depends on the difference between these two power values. In other words, if the power injected into the grid is higher than the power generated by the WT for a long time, all the MMSHC batteries will be discharged to their lower limits. Moreover, there is also a limit of time in which the power generated by the WT can be higher than the power injected into the grid by the MMSHC, and this time depends on the difference between these two power values. In other words, if the power generated by the WT is higher than the power injected into the grid for a long time, all the MMSHC batteries will be charged to their upper limits. Whenever one of these limits

are reached, either the MMSHC grid-side or load-side power set point must be changed. As will be explained in detail in the Simulation Results section, when the grid-side power is higher than the machine-side power for a long time, or vice versa, the frequency of operation of the MMSHC swap switches increases as the SOC values of the batteries come close to the previously mentioned upper and lower limits. Thus, the moment of changing either the grid-side or load-side power set points is defined according to a desirable limit of switching-frequency operation of the swap switches. The detailed explanation of the last stage of the MMSHC control will be provided in the Simulation Results section later in this paper.

IV. Simulation Results

In this section, simulation results are presented in which the proposed MMSHC (see Fig. 1) drives a permanent-magnet-synchronous generator (PMSG), emulating a WT. The system is connected to a 5-kV, 50-Hz grid. The generator presents rated power equal to 3 MVA, rated voltage equal to 10 kV (line-to-line) and rated frequency equal to 60 Hz. Each string is composed of four FB submodules ($N = 4$) with IGBTs and each FB submodule has its own integrated battery pack. These battery packs present a rated voltage equal to 1 kV, rated capacity equal to 0.125 Ah and initial SOC value equal to 60%. In this analysis, an extremely low battery-energy value was used so that it was possible to analyze the MMSHC behavior in 15 s of simulation. In this simulation, the swap switches are bidirectional switches. The LSC-PWM technique is adopted with a carrier frequency equal to 5 kHz. The generator regulation is based on a flux-oriented-control (FOC) technique, as illustrated in Fig. 7, in which the machine current (i_l) is controlled in a rotating reference frame aligned with the rotor flux (θ_R). Thus, by controlling the direct-axis current component (i_{ld}), it is possible to control the machine reactive power, whereas by controlling the in-quadrature-axis current component (i_{lq}), it is possible to control the machine angular speed (ω_R). The FOC control generates the voltage reference (v^*_{labc}) that is provided to the converter internal control depicted in Fig. 6.

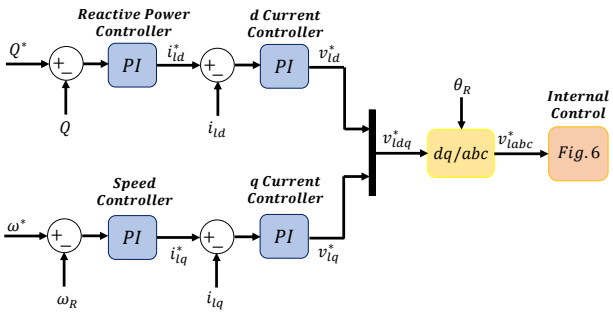

Fig. 7. Generator control.

A. Operation Without Changing Power Set Points

The first simulation carried out shows the operation of the MMSHC when no change in its grid-side and load-side power set points is required. In other words, neither the grid-side power is kept higher than the load-side power for a long time, nor the load-side power is kept higher than the grid-side power for a long time. In this simulation, the grid-side voltage control, responsible for generating the voltage reference (v^*_{gabc}), is executed in an open-loop fashion. In other words, a voltage reference with fixed amplitude, which is equal to the grid-voltage amplitude, and a small phase shift in relation to the grid voltage, is provided to the converter internal control shown in Fig. 6. The small phase shift is the one necessary to obtain a fixed value of the active power injected into the grid (P_g), which is equal to approximately 1.05 MW. In Fig. 8 and Fig. 9, simulation results obtained with the software PSCAD/EMTDC can be observed. At $t = 0.5$ s, the generator is started receiving a speed reference equal to $\omega^* = 0.2$ pu and receiving as an input a mechanical torque with a value equal to 1.4 pu. At $t = 4$ s, the generator speed reference changes from 0.2 pu to 0.3 pu. At $t = 8$ s, the wind speed increases, resulting in an increase of the generator mechanical torque that changes from 1.4 pu to 1.8 pu. In Fig. 8(a) and (b), the load-side and grid-side multilevel voltages can be observed, respectively. These two voltages can be controlled in an independent fashion. In Fig. 8(c), the load-side power (P_l) and the grid-side power (P_g) are shown. Initially, the load-side power (P_l) is lower than the grid-side power (P_g). At $t = 4$ s, when the generator speed increases, the load-side power increases, and it becomes slightly higher than the grid-side one. At $t = 8$ s, when the mechanical torque increases, the load-side power becomes considerably higher than the grid-side power. In Fig. 8(d), one can observe the generator angular speed (ω_R) and it is clear that the MMSHC is capable to properly track the angular-speed reference with values $\omega^* = 0.2, 0.3$ pu.

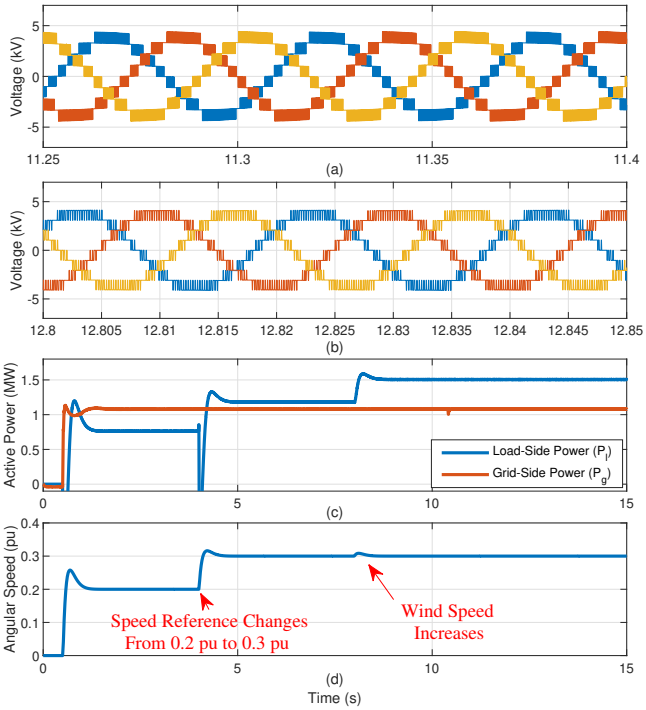

Fig. 8. Simulation results. (a) Load-side voltage, (b) grid-side voltage, (c) load-side and grid-side power and (d) machine angular speed.

In Fig. 9(a), (c) and (e), the battery-SOC values of String X phases A, B and C are shown, respectively. In Fig. 9(b),

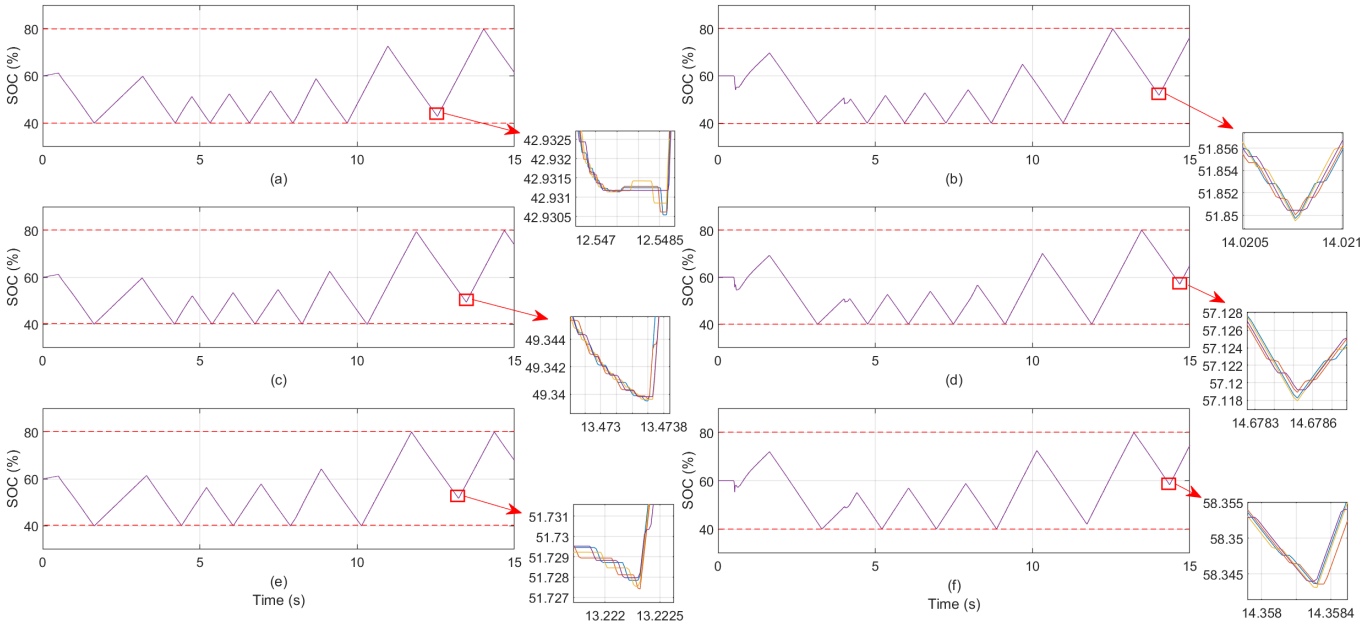

Fig. 9. Battery-SOC profiles. (a) Phase-A string X, (b) phase-A string Y, (c) phase-B string X, (d) phase-B string Y, (e) phase-C string X and (f) phase-C string Y.

(d) and (f), the battery-SOC values of String Y phases A, B and C are shown, respectively. As described in Fig. 6, the battery SOC of all the MMSHC submodules are controlled to vary within a pre-defined range (between the pre-defined upper and lower SOC limits). In this analysis, the upper SOC limit was set to 80% and the lower SOC limit was set to 40%. By analyzing Fig. 9, it is clear that the proposed control algorithm (see Fig. 6) is capable to maintain the battery SOC of all the MMSHC submodules within the desired limits, during the entire simulation period considered. Besides, by observing the zoom in the battery-SOC signals, it is clear that the SOC-balancing control is working properly since all the submodules within the same string remain with similar battery-SOC values (see zooms in Fig. 9). By analyzing Fig. 8 and Fig. 9, one can notice that during the period in which the load-side power (P_l) is lower than the grid-side power (P_g), before $t = 4$ s, all the batteries are discharged, in average, and every time the battery-SOC values of a given string reach the lower limit equal to 40%, the swap switches act connecting this string to the generator terminals and connecting its complementary string to the grid terminals. The average reduction of the battery-SOC values occurs because the batteries of the strings connected to the grid are being discharged at a higher rate than the batteries of the strings connected to the generator are being charged. On the other hand, when the load-side power (P_l) is higher than the grid-side power (P_g), after $t = 4$ s, all the batteries are charged, in average, and every time the battery-SOC values of a given string reach the upper limit equal to 80%, the swap switches act connecting this string to the grid terminals and connecting its complementary string to the generator terminals. The average increase of the battery-SOC values occurs because the batteries of the strings connected to the generator are being charged at a higher rate than the batteries of the strings connected to the grid are being discharged. One important issue to be observed is that, before $t = 4$ s, when the batteries are being discharged in average, as closer to the lower limit the battery-SOC values of a given phase come, faster the operation of the swap switches is. In other words, these devices will switch more often as closer to the lower limit the battery-SOC values are. This fact happens because, as previously mentioned, the battery-SOC values are being reduced, in average, and, thus, it takes less time for the discharging batteries to reach the lower SOC limit. Of course that, in this paper, an extremely low battery-energy value was used so that it was possible to analyze the MMSHC behavior in 15 s of simulation. In a real application, the battery energy should be much higher in such a way that the swap-switch switching could occur in a scale of minutes. The increase in the frequency of operation of the swap switches is the reason why the last stage of the MMSHC internal control named "Limitation of Swap-Switch Switching Frequency" (see Fig. 6) is required. The last stage of the control will be explained in the next two subsections.

In Fig. 10 (a) and (b), the battery SOC of each submodule within phase-A String X and phase-A String Y is shown, respectively. In Fig. 10 (c) and (d), the battery power of each submodule within phase-A String X and phase-A String Y is shown, respectively. Fig. 10 is interesting because it illustrates the switching frequency of the swap switches and of the FB submodules. In other words, the swapping action only occurs when the battery SOC of either String X or String Y reaches either the upper SOC limit or the lower SOC limit. This operation defines the switching frequency of the swap switches that is extremely low as observed in Fig. 10 (a) and (b). The operation of the FB submodules, however, occurs with the sampling frequency of the control algorithm

(illustrated in Fig. 6). In this simulation, the control algorithm runs with a sampling frequency equal to 20 kHz, which means that, every 50 μs, the sorting algorithm decides a new set of submodules to be inserted and to be by-passed, maintaining the battery-SOC balance of the submodules within the same string. For example, by observing Fig. 10 (a), one can see the zoom in the battery-SOC values of the four submodules within phase-A String X and it is clear that, while the battery-SOC values of some submodules are increasing, because these submodules are inserted, the battery-SOC values of other submodules are kept constant, because these submodules are by-passed. In other words, every 50 μs, different submodules are selected to be inserted and to be charged. This fact can be confirmed by analyzing the battery power values, shown in Fig. 10 (c), which illustrate that, every 50 μs, a new set of batteries are being charged, with positive power values, since their corresponding submodules are inserted. The by-passed submodules present instantaneous battery power equal to zero. It is also interesting to notice that, during the moments in which the batteries of String X are being charged (with increasing SOCs and with positive power values as illustrated in Fig. 10 (a) and (c), respectively), the batteries of String Y are being discharged (with decreasing SOCs values and with negative power values as illustrated in Fig. 10 (b) and (d), respectively). This operation mode is over when the swapping action occurs. Obviously, the switching frequency of the FB submodules is imposed by the sampling frequency of the control algorithm, which is quite high in this simulation (equal to 20 kHz). In a real application, the frequency of the SOC-balancing control could be limited to reduce the switching frequency of the FB submodules. It is, of course, a trade-off between improving the SOC balance and reducing the switching losses. However, since the time constant of the battery SOC is large, then, in a real application, the frequency of the sorting algorithm could, indeed, be small and still proper battery-SOC balance would be obtained. This way, the solution would operate with low switching frequency and low switching losses.

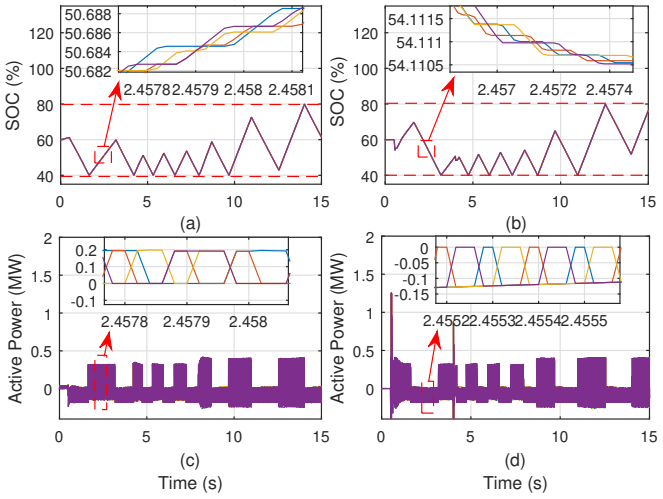

Fig. 10. (a) Battery SOC of each submodule within Phase-A String X, (b) battery SOC of each submodule within Phase-A String Y, (c) battery power of each submodule within Phase-A String X and (d) battery power of each submodule within Phase-A String Y.

B. Reduction of Grid-Side Power Set Point

The simulation carried out in this subsection is based on the exact same parameters as the simulation carried out in the previous subsection, however, in this case, the grid-side power (P_g) is kept considerably higher than load-side power (P_l) for a long time and, thus, a reduction of the grid-side-power set point will be required in order to avoid that the swap-switch switching frequency becomes too high. In this simulation, the load-side power (P_l) is kept fixed with value equal to 0.75 MW through the entire simulation period. The grid-side power (P_g) starts with a set point equal to 1.05 MW. The MMSHC power values can be seen in Fig. 11(c). Obviously, the grid-side power is considerably higher than the load-side power and, as expected, the battery-SOC values of all the MMSHC strings will be discharged, in average, along time. In Fig. 11(a) and (b), the battery SOCs of the submodules in Strings X and Y of the MMSHC phase B are depicted, respectively. It is clear that the battery-SOC values of both strings are decreasing, in average, along time. Moreover, it is also clear that as the SOC values are reduced along time, the swap switches start to operate more often. Thus, according to the last stage of the control shown in Fig. 6, when the battery-SOC values of the submodules in both strings become, simultaneously, smaller than a pre-defined limit equal to the lower limit plus an extra delta value (Δ_{SOC}), then the grid-side-power set point should be reduced, as the batteries cannot be discharged any longer. In this analysis, the lower SOC limit is equal to 40% and the delta SOC value is equal to $\Delta_{SOC} = 2\%$ and, thus, the limit of SOC that both the strings need to reach, simultaneously, so that the grid-side-power set point must be changed is equal to 42%.

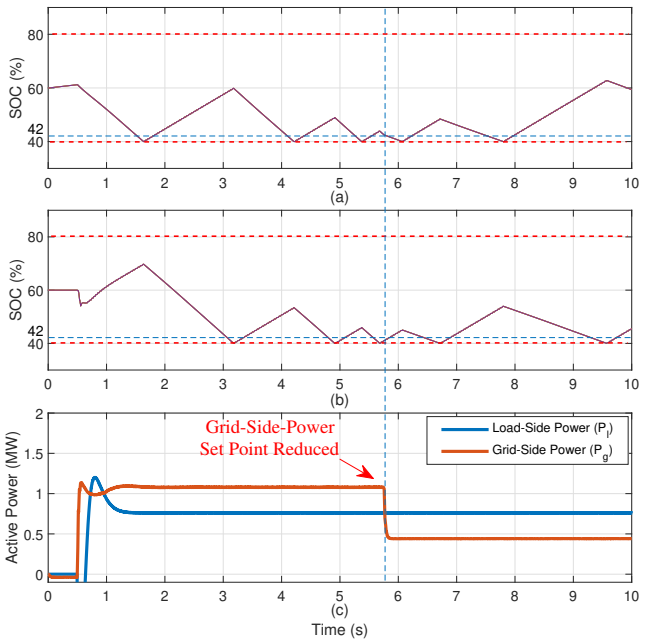

Fig. 11. (a) Battery SOC of string X of Phase B, (b) battery SOC of string Y of Phase B and (c) MMSHC grid-side power and load-side power.

In Fig. 11(a) and (b), horizontal dashed lines with the red color are used to highlight the upper and lower SOC limits equal to 80% and 40%, respectively. Moreover, horizontal

dashed lines with the blue color are used to illustrate the limit equal to 42% that corresponds to the power-set-point-change limit. The moment highlighted by the vertical dashed line corresponds to the instant in which the battery-SOC values of both strings (X and Y) are, simultaneously, smaller than the 42% limit for the first time. At this moment, the grid-side power set point is reduced to a value lower than the load-side power because the MMSHC batteries can no longer be discharged. The 42% limit could be higher (45% for example) in order to limit even further the swap-switch switching frequency. Obviously, after the grid-side power set point is reduced, the MMSHC batteries start to charge, in average, and the frequency of operation of the swap switches starts to decrease. The reason why only Strings X and Y of phase B are shown in Fig. 11 is because this is the first phase to cross the 42% limit and, thus, the one that leads to the grid-side power-set-point reduction.

C. Reduction of Load-Side Power Set Point

The simulation carried out in this subsection is based on the exact same parameters as the ones carried out in the previous two subsections, however, in this case, the load-side power (P_l) is kept considerably higher than grid-side power (P_g) for a long time and, thus, a reduction of the load-side power set point will be required in order to avoid that the swap-switch switching frequency becomes too high. The grid-side power (P_g) is kept fixed with a value equal to 0.5 MW during the entire simulation period. Initially, the machine-speed set point is equal to $\omega^* = 0.2$ pu, which results in a load-side power (P_l) equal to approximately 1.05 MW. The simulation results obtained are depicted in Fig. 12. Since the load-side power is considerably higher than the grid-side power, as expected the battery-SOC values of all the MMSHC strings will be charged, in average, along time. In Fig. 12(a) and (b), the battery SOCs of the submodules in Strings X and Y of the MMSHC phase C are depicted, respectively. It is clear that the battery-SOC values of both strings are increasing, in average along time. Moreover, it is also clear that as the SOC values are increased along time, the swap switches start to operate more often. Thus, according to the last stage of the control shown in Fig. 6, when the battery-SOC values of the submodules in both strings become, simultaneously, bigger than a pre-defined limit equal to the upper limit minus the previously-defined delta value (Δ_{SOC}), then the load-side power set point should be reduced, as the batteries cannot be charged anymore. In this analysis, the upper SOC limit is equal to 80% and the delta SOC value is equal to $\Delta_{SOC} = 2\%$ and, thus, the limit of SOC that both the strings need to reach, simultaneously, so that the load-side power set point must be changed is equal to 78%. In Fig. 12(a) and (b), horizontal dashed lines with the red color are used to highlight the the upper and lower SOC limits equal to 80% and 40%, respectively. Moreover, horizontal dashed lines with the blue color are used to represent the limit equal to 78% that corresponds to the power-set-point-change limit. The moment highlighted by the vertical dashed line corresponds to the instant in which the battery-SOC values of both strings (X and Y) are, simultaneously, bigger than the 78% limit for the first time. At this moment, the load-side power set point is reduced to a value lower than the grid-side power because the MMSHC batteries can no longer be charged. In order to reduce the load-side power, the machine speed should be controlled to a lower value. Thus, at the moment highlighted by the vertical dashed line, the machine angular-speed reference changes from $\omega^* = 0.2$ pu to $\omega^* = 0.05$ pu, as illustrated in Fig. 12(c), which results in the load-side-power reduction shown in Fig. 12(d). The 78% limit could be lower (75% for example) to limit even further the swap-switch switching frequency. Obviously, after the load-side power set point is reduced, the MMSHC batteries start to discharge, in average, and the frequency of operation of the swap switches starts to decrease. The reason why only Strings X and Y of phase C are shown in Fig. 12 is because this is the first phase to cross the 78% limit and, thus, the one that leads to the load-side power set-point reduction.

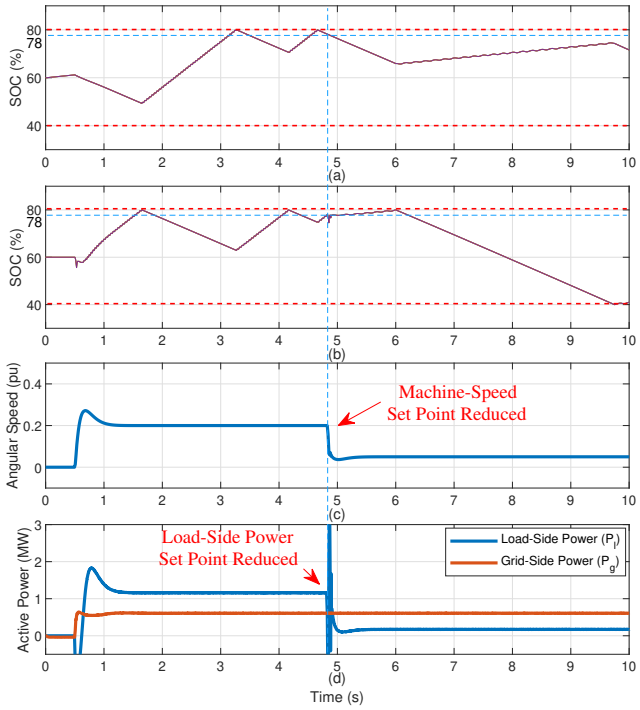

Fig. 12. (a) Battery SOC of string X of Phase C, (b) battery SOC of string Y of Phase C, (c) machine angular speed and (d) MMSHC grid-side power and load-side power.

D. Detailed Analysis of Mechanical-Swap-Switch Snubber-Circuit Operation

In the previous simulations, the swap switches were considered to be bidirectional switches operating with a four-step commutation method. In this subsection, a simulation analysis is carried out to demonstrate the detailed operation of the snubber circuit of the swap switches if they are mechanical ones. In order to be possible to utilize mechanical swap switches, a considerably high dead time must be adopted since the mechanical switches can take, typically, at least 10 ms to both turn on and turn off. Thus, in this simulation, a dead time equal to 50 ms was adopted. The snubber circuit used is the one illustrated in Fig. 4. This is a RC circuit with

resistance equal to $0.1\ \Omega$ and capacitance equal to $4\ \mu$F. Nonetheless, it is important to emphasize that proposing the most efficient circuit to divert the inductive current during the dead time is not the main focus of this paper. Other snubber-circuit configurations or clamping circuits could eventually be adopted and could even be more efficient and more suitable options.

In Fig. 13(a) and (b), one can observe the battery SOCs of phase-A String X and phase-A String Y, respectively. As expected, one submodule string is kept connected to the grid terminal and the other is kept connected to the generator terminal while the battery-SOC values vary within a pre-defined range. Every time either the upper SOC limit (equal to 80%) or the lower SOC limit (equal to 40%) is reached by the batteries of any of the two strings, then the swapping action occurs, which means that the submodule string that was connected to the grid terminal (discharging) is then connected to the generator terminal, and the submodule string that was connected to the generator terminal (charging) is then connected to the grid terminal. In Fig. 13(c), the switching states of the swap switches that connect the phase-A String X to the grid terminal and to the generator terminal (S_{XA} and S_{Xa}, respectively) are shown, in which 1 means on state and 0 means off state. By analyzing the switching states, one can notice that the swapping action occurs, in fact, every time the battery SOC of any of the strings reach the upper limit equal to 80%. Moreover, by analyzing the zoom in the switching-state signals, one can observe the dead-time period in which both swap switches are in off state. It is clear that the dead time is, in fact, equal to 50 ms. In Fig. 13(d) and (e), the snubber-circuit current (i_{snub}) and voltage (v_{snub}) of the swap switch that connects the phase-A String X to the grid terminal are shown, respectively.

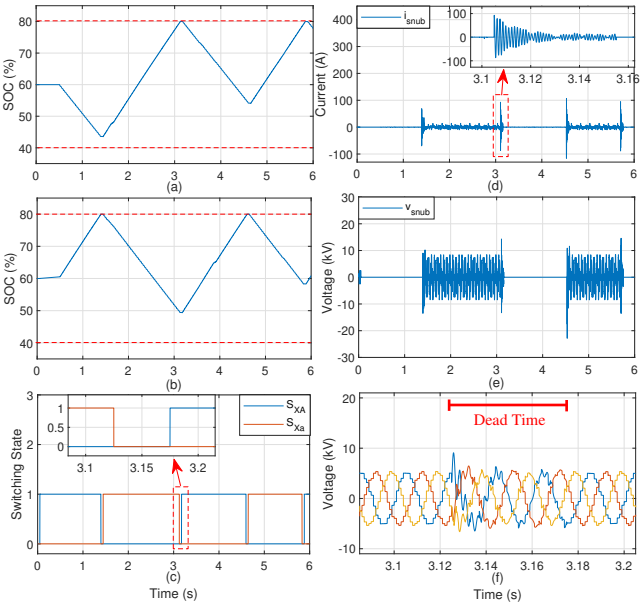

Fig. 13. a) Battery SOC of Phase-A string X, (b) battery SOC of Phase-A string Y, (c) switching state of swap switches that connect phase-A String X to grid and generator terminals (S_{XA} and S_{Xa}), (d) snubber-circuit current of swap switch that connects phase-A String X to grid terminal (i_{snub}), (e) snubber-circuit voltage of swap switch that connects phase-A String X to grid terminal (v_{snub}) and (f) voltages synthesized at the grid terminals.

The snubber-circuit current and voltage that are measured in the simulation are described in detail in Fig. 4. The snubber current (i_{snub}) is basically null throughout most of the simulation period. During the dead time of the swapping action, however, current flows through the snubber circuit as expected. The snubber circuit absorbs the peak current that occurs when the inductive current is cut. After this transient moment, a smaller current keeps flowing through the snubber circuit until the dead-time period is over. It is obvious that the losses in the snubber circuit are quite low since current only flows through it during the dead time of the swapping action and, especially, because the swapping action only occurs occasionally in the proposed converter solution with integrated batteries. In this simulation, an extremely low battery energy was considered to demonstrate the operation of the swap-switch snubber circuit within 6 s of simulation. In a real application, however, the battery energy should be much higher in a way that the swapping action would occur quite rarely, in a scale of several minutes. The voltage across the snubber circuit (v_{snub}) is either null (if the swap switch is in conducting mode) or it is equal to the difference between the voltages synthesized by String X and String Y (if the swap switch is in blocking mode). During the dead-time period, the grid and generator voltages become distorted as illustrated in Fig. 13(f) that shows the voltages synthesized at the grid terminals during the dead-time period. Once again, it is important to highlight that, in a real application, these undesired transient moments would only occur occasionally since the swapping action would only happen when the submodule-string batteries were charged or discharged to their SOC limits (every several minutes). Nonetheless, it is true that depending on the snubber-circuit design, overvoltages and harmonic distortion above the allowed limits might occur in the voltage synthesized at the grid terminals. Thus, designing a proper circuit to divert the inductive current during the commutation is essential for the proper performance of the MMSHC with mechanical swap switches. Probably, adopting the bidirectional-switch-based swap switches could be a better option to make the MMSHC become a competitive industrial solution.

V. Experimental Validation

In order to validate the proposed MMSHC, an experimental prototype was built as shown in Fig. 14. The test setup is composed of two strings of FB submodules (String 1 and String 2), two swap circuits (Swap 1 and Swap 2) and two 5-mH inductors (L_1 and L_2). Each string is composed of three FB submodules ($N = 3$). DC voltage sources (DC power supplies) are connected to each submodule in order to represent the batteries. Each swap circuit is composed of two bidirectional switches with individual snubber circuits for safety reasons. A resistive load ($R = 12\ \Omega$) is connected to each terminal of the converter. In this experimental test, the DC voltage sources are set with a 20-V value and the voltage control of both strings is executed in an open-loop fashion tracking a voltage reference with fixed amplitude equal to 60 V. The LSC-PWM technique is used with a 10-kHz carrier frequency. The experimental results prove that the MMSHC is capable

to synthesize two independent AC voltages, operating as a controlled voltage source from both grid and load perspectives. Moreover, the experimental results validate the operation of the swap switches. A diagram illustrating the experimental-setup details is depicted in Fig. 15.

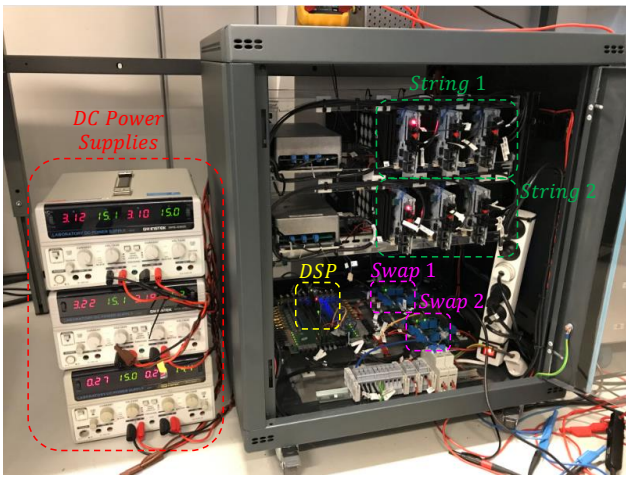

Fig. 14. Experimental prototype.

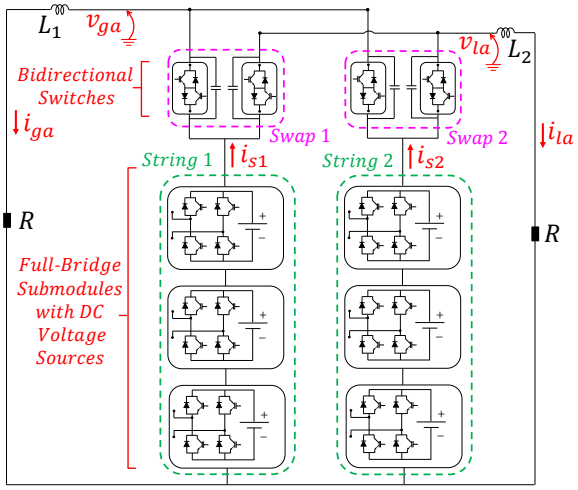

Fig. 15. Experimental prototype diagram.

First, the operation of the swap switches is tested. A dead-time technique was implemented in order to avoid a short circuit between strings. Moreover, snubber circuits are used to create a path for the inductive currents to flow through during the dead-time period of the swap-switch commutation. So, every time a swapping command is provided, first, all the swap switches in on state receive the turn-off signal. Next, a dead-time period is introduced and, finally, the turn-on signal is provided to the swap switches to be closed. In the experimental results shown in Fig. 16, the voltage synthesized at both terminals (two upper signals) can be seen, which are signals with an amplitude equal to 60 V and frequency equal to 50 Hz. The two lower signals shown in Fig. 16 are the String 1 and String 2 currents (i_{s1} and i_{s2} according to Fig. 15). The inductor of one terminal (L_2) was removed to observe the swapping operation. In other words, for half of a period, the string currents present the multilevel shape as they are flowing into the terminal in which the inductor has been removed, while for the next half of a period the currents are sinusoidal signals, as they flow into the terminal with the inductor, which filters out the high-order-harmonic components present in the voltage waveform. It means that the submodule strings are swapping and, every half of a period, they are connected to a different terminal. The swap switches operate with 100 Hz, as visible in the current commutation in Fig. 16. It is important to notice that the voltages at both terminals remain regulated, according to their references, even though each of them is synthesized by a different submodule string every half of a period. In Fig. 17, it is possible to observe the operation of the MMSHC while synthesizing voltages with different frequencies at each terminal, which would be the natural condition in a WT application. In Fig. 17, the frequency of the signal v_{ga} is equal to 50 Hz, whereas the frequency of the signal v_{la} is equal to 10 Hz. Both inductors L_1 and L_2 are connected in this case, in such a way that the currents i_{ga} and i_{la} (two lower signals in Fig. 17) are filtered signals. It is clear that the converter is capable of synthesizing independent voltages with different frequencies at each converter terminal.

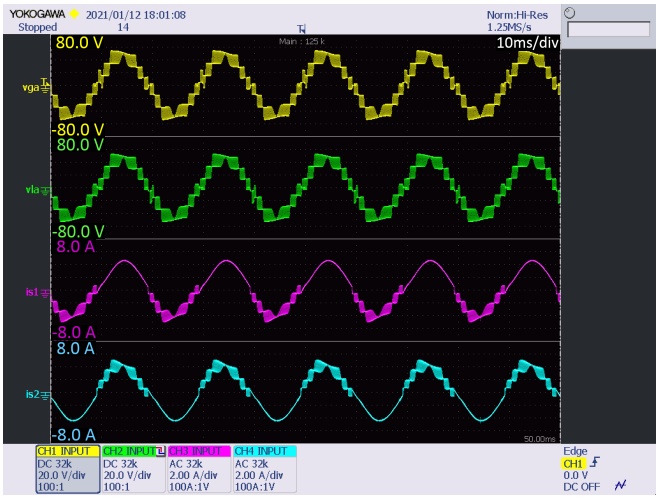

Fig. 16. From top to bottom. First signal: Voltage v_{ga}, second signal: Voltage v_{la}, third signal: Current i_{s1} and fourth signal: Current i_{s2}.

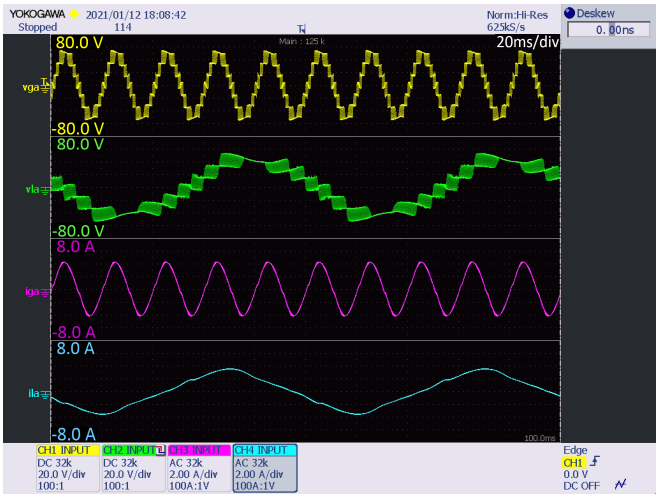

Fig. 17. From top to bottom. First signal: Voltage v_{ga}, second signal: Voltage v_{la}, third signal: Current i_{ga} and fourth signal: Current i_{la}.

VI. Conclusion

In this paper, a new converter solution named modular multilevel shunt converter was proposed. This new topology allows for a straightforward integration with batteries into the same converter that drives the WT. Due to its modular multilevel structure, the proposed converter solution can be used to drive modern high-power medium-voltage WTs and these WTs can operate with high flexibility and in a dispatchable fashion benefiting both the power system operator and the wind-power-plant owner. To the best of the authors' knowledge, the proposal of a converter topology with modular multilevel structure and battery integration used to drive a MV WT, operating with different grid-side and generator-side power set points, is a topic rarely or never explored in the literature before. In this paper, simulation analyses were carried out, through the software PSCAD/EMTDC, with the MMSHC driving a PMSG representing a WT. The system was simulated with different grid-side and generator-side power set points in which the batteries absorbed/supplied the power mismatches between grid and generator terminals. Finally, experimental results were presented to validate the MMSHC behavior as independent controlled voltage sources capable to synthesize different voltages at the grid and at the load terminals and to validate the operation of the swap switches.

References

[1] L. Qu and W. Qiao, "Constant power control of DFIG wind turbines with supercapacitor energy storage," *IEEE Transactions on Industry Applications*, vol. 47, no. 1, pp. 359–367, 2011.

[2] L. Miao, J. Wen, H. Xie, C. Yue, and W. J. Lee, "Coordinated Control Strategy of Wind Turbine Generator and Energy Storage Equipment for Frequency Support," *IEEE Transactions on Industry Applications*, vol. 51, no. 4, pp. 2732–2742, 2015.

[3] C. L. Moreira, F. O. Resende, and J. A. Lopes, "Using low voltage MicroGrids for service restoration," *IEEE Transactions on Power Systems*, vol. 22, no. 1, pp. 395–403, 2007.

[4] P. Pinson, "Wind energy: Forecasting challenges for its operational management," *Statistical Science*, vol. 28, no. 4, pp. 564–585, 2013.

[5] N. Fichaux, J. Beurskens, P. H. Jensen, J. Wilkes, S. Frandsen, J. D. Sorensen, P. Eecen, C. Malamatenios, J. A. Gomez, J. Hemmelmann, G. van Kuik, B. Bulder, F. Rasmussen, B. Janssen, T. Fischer, E. Bossanyi, M. Courtney, J. Giebhardt, R. Barthelmie, O. Holmstrom, D. Iuga, and S. Wokke, "UPWIND - Design Limits and Solutions for Very Large Wind Turbines," 2011.

[6] M. Diaz, R. Cárdenas, M. Espinoza, A. Mora, and P. Wheeler, "Modelling and control of the modular multilevel matrix converter and its application to wind energy conversion systems," in *IECON 2016 - 42nd Annual Conference of the IEEE Industrial Electronics Society*, Florence, 2016.

[7] A. Madariaga, J. L. Martín, I. Zamora, I. Martínez De Alegría, and S. Ceballos, "Technological trends in electric topologies for offshore wind power plants," *Renewable and Sustainable Energy Reviews*, vol. 24, pp. 32–44, 2013.

[8] T. M. Iversen, S. S. Gjerde, and T. Undeland, "Multilevel converters for a 10 MW, 100 kV transformer-less offshore wind generator system," *2013 15th European Conference on Power Electronics and Applications, EPE 2013*, pp. 1–10, 2013.

[9] M. Diaz, R. Cardenas, M. Espinoza, F. Rojas, A. Mora, J. C. Clare, and P. Wheeler, "Control of Wind Energy Conversion Systems Based on the Modular Multilevel Matrix Converter," *IEEE Transactions on Industrial Electronics*, vol. 64, no. 11, pp. 8799–8810, 2017.

[10] ABB, *PCS 6000 for large wind turbines Medium voltage, full power converters up to 9 MVA*, 2012. [Online]. Available: https://new.abb.com/docs/default-source/ewea-doc/pcs6000wind.pdf?sfvrsn=2

[11] S. K. Chaudhary, A. F. Cupertino, R. Teodorescu, and J. R. Svensson, "Benchmarking of modular multilevel converter topologies for ES-STATCOM realization," *Energies*, vol. 13, no. 13, pp. 1–22, 2020.

[12] M. Vasiladiotis and A. Rufer, "Analysis and control of modular multilevel converters with integrated battery energy storage," *IEEE Transactions on Power Electronics*, vol. 30, no. 1, pp. 163–175, 2015.

[13] N. Kawakami, S. Ota, H. Kon, S. Konno, H. Akagi, H. Kobayashi, and N. Okada, "Development of a 500-kW modular multilevel cascade converter for battery energy storage systems," *IEEE Transactions on Industry Applications*, vol. 50, no. 6, pp. 3902–3910, 2014.

[14] J. I. Y. Ota, T. Sato, and H. Akagi, "Enhancement of performance, availability, and flexibility of a battery energy storage system based on a modular multilevel cascaded converter (MMCC-SSBC)," *IEEE Transactions on Power Electronics*, vol. 31, no. 4, pp. 2791–2799, 2016.

[15] S. D'Arco, M. Quraan, P. Tricoli, and L. Piegari, "Low Frequency Operation of Modular Multilevel Converters with Embedded Battery Cells for Traction Drives," *International Symposium on Power Electronics, Electrical Drives, Automation and Motion*, pp. 1375–1382, 2016.

[16] C. Zhang, D. Jiang, X. Zhang, J. Chen, C. Ruan, and Y. Liang, "The Study of a Battery Energy Storage System Based on the Hexagonal Modular Multilevel Direct AC/AC Converter (Hexverter)," *IEEE Access*, vol. 6, pp. 43 343–43 355, 2018.

[17] D. Sera, L. Mathe, and M. Ricco, "Flexible and efficient switched string converter," International Patent - World Intellectual Property Organization/Patent Cooperation Treaty (WIPO/PCT) WO 2020/043 258 A1, Mar. 05, 2020.

[18] J. W. Baek, D.-w. Yoo, and H.-g. Kim, "High-Voltage Switch Using Series-Connected IGBTs With Simple Auxiliary Circuit," *IEEE Transactions on Industry Applications*, vol. 37, no. 6, pp. 1832–1839, 2001.

[19] P. W. Wheeler, J. Rodríguez, J. C. Clare, L. Empringham, and A. Weinstein, "Matrix converters: A technology review," *IEEE Transactions on Industrial Electronics*, vol. 49, no. 2, pp. 276–288, 2002.

[20] Z. Malekjamshidi, M. Jafari, J. Zhang, and J. Zhu, "Design and Analysis of Protection Circuits for Safe Operation of Direct Matrix Converters," *2017 20th International Conference on Electrical Machines and Systems, ICEMS 2017*, pp. 0–3, 2017.

[21] V. Pala, E. V. Brunt, L. Cheng, M. O'Loughlin, J. Richmond, A. Burk, S. T. Allen, D. Grider, J. W. Palmour, and C. J. Scozzie, "10 kV and 15 kV silicon carbide power MOSFETs for next-generation energy conversion and transmission systems," *2014 IEEE Energy Conversion Congress and Exposition, ECCE 2014*, pp. 449–454, 2014.

[22] K. Sharifabadi, L. Harnefors, H.-P. Nee, S. Norrga, and R. Teodorescu, *Design, Control, and Application of Modular Multilevel Converters for HVDC Transmission Systems*. John Wiley & Sons, 2016.